A novel oncogenic enhancer of estrogen receptor-positive breast cancer

Chunjie Bao,[1,3] Jialun Duan,[1,2,3] Ying Xie,[1,3] Yixuan Liu,[1] Peishan Li,[1] Jianwei Li,[1] Huihui Zhao,[1] Haitao Guo,[1] Yanchen Men,[1] Yuxin Ren,[1] Jiarui Xu,[1] Guiling Wang,[1] and Wanliang Lu[1]

[1]State Key Laboratory of Natural and Biomimetic Drugs, Beijing Key Laboratory of Molecular Pharmaceutics and Drug Delivery Systems, School of Pharmaceutical Sciences, Peking University, Beijing 100191, China; [2]College of Pharmacy, Jiangsu Provincial TCM Engineering Technology Research Center of High Efficient Drug Delivery System (DDS), Nanjing University of Chinese Medicine, Nanjing 210023, China

Estrogen receptor-positive (ER$^+$) breast cancer accounts for the majority of breast cancers diagnosed, and nearly 20% of patients do not respond to endocrine therapy. The pathogenesis of ER$^+$ breast cancer has not been well elucidated. The enhancer is a *cis*-regulatory element that promotes gene transcription and plays an important role in the spatiotemporal expression of cellular genes. Nevertheless, the oncogenic enhancer and its role in the occurrence and progression of cancer remain unclear. Here, we report a novel oncogenic enhancer (named αE_{myc}) for *c-Myc* and reveal its activation mechanism in ER$^+$ breast cancer. The results demonstrated that αE_{myc} enhanced the transcription of downstream genes more than 20-fold. The deletion of the 7-bp region (*GGT TGCA*) in αE_{myc} significantly downregulated the expression of *c-Myc*, resulting in cell nuclear changes, cell-cycle arrest, cell apoptosis, and finally, remarkable inhibition of cell proliferation. In conclusion, the present study discovers a novel oncogenic enhancer αE_{myc} (801 base pairs [bp], at Chr8: 127668529–127669329) and offers a remarkable core enhancer target (*GGTTGCA*) of αE_{myc} for gene therapy of ER$^+$ breast cancer.

INTRODUCTION

Enhancers have gradually been recognized as functional noncoding DNA sequences, which are *cis*-regulatory elements that can remarkably promote gene transcription in a specific cell or tissue. The enhancer is located at the 5′ or 3′ end of a specific gene and exists at the sequence either near the promoter of the target gene or thousands of base pairs (bp) away from the target gene.[1] With the participation of cofactors such as histone acetyl transferases, topological changes in chromatin occur, forming a three-dimensional DNA-loop structure. Such a structure shortens the spatial distance between the enhancer and promoter, thereby inducing the recruitment of transcription factors such as RNA polymerase II (RNA Pol II) to stimulate the transcription of target genes. To some extent, an enhancer could increase the transcription level of a specific gene by 10–1,000 times.

It is known that enhancers are able to regulate the precise spatiotemporal patterns of gene expression during cell development.[2–4]

Furthermore, enhancers may also be involved in tumorigenesis.[5–8] Previous investigations showed that the activated enhancers of oncogenes in a tumor-specific environment could drive the uncontrolled growth and metastasis of cancers.[7,9–11] Nevertheless, the oncogenic enhancer itself and its role in the occurrence and progression of cancer are not understood.

Here, we report a novel oncogenic enhancer (named αE_{myc}) that plays a major role in the proliferation of estrogen receptor-positive (ER$^+$) breast cancer cells by promoting the transcription of *c-Myc*. We further reveal the clinical significance of the finding that this oncogenic enhancer could be a remarkable treatment target for this type of cancer.

Breast cancer is the leading type of cancer in women worldwide, accounting for 19.9% of all cancer cases.[12] Based on the expression of three receptors, ER, progesterone receptor (PR), and human epidermal growth factor receptor 2 (HER2), breast cancer can be classified into ER$^+$ breast cancer cells, HER2$^+$ breast cancer cells, and triple-negative breast cancer cells.[13,14]
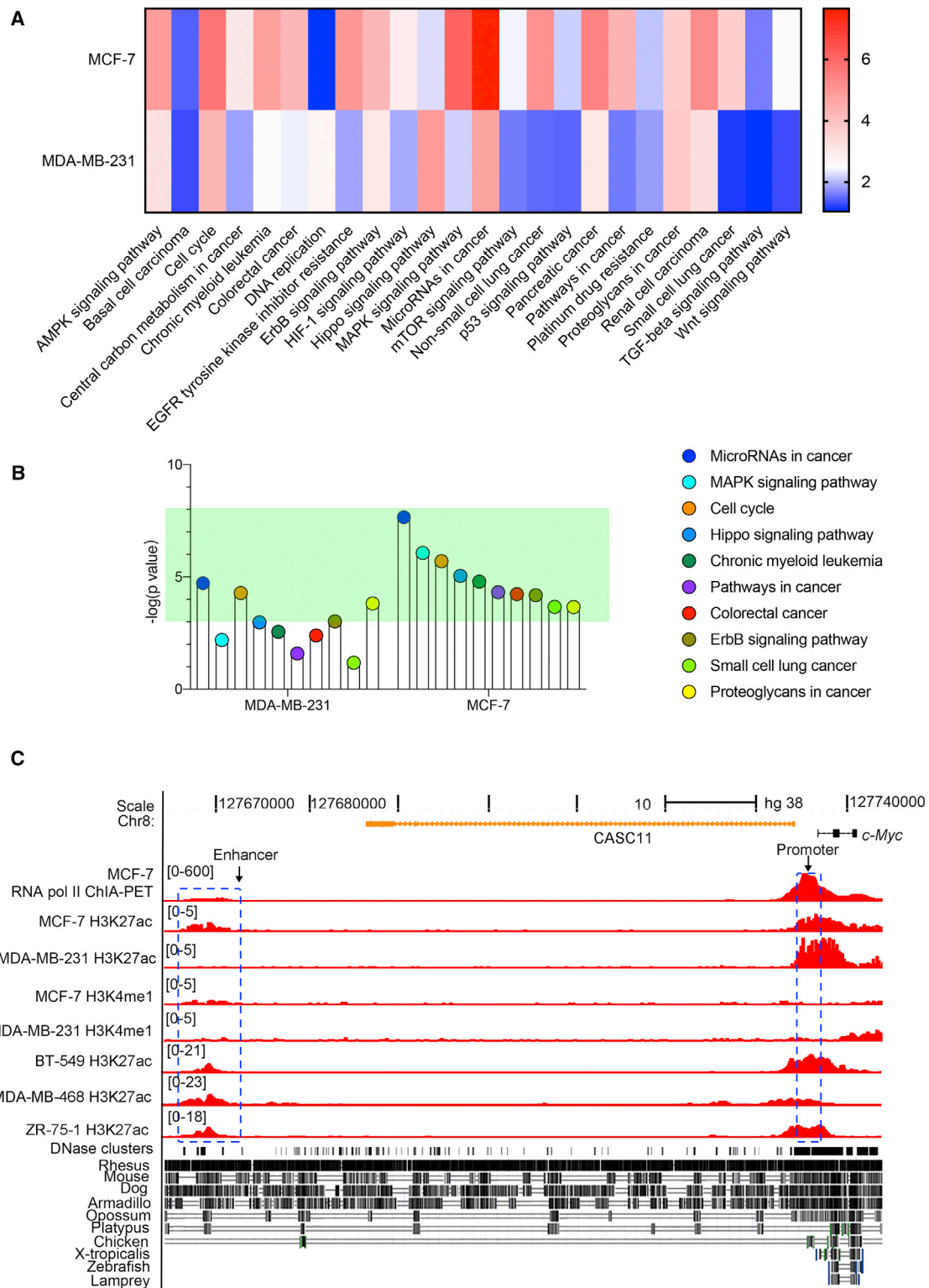
ER$^+$ breast cancer accounts for approximately 79% of all breast cancers diagnosed.[15] Clinically, patients with ER$^+$ breast cancer are basically treated with drugs (e.g., tamoxifen) to block estrogen effects (endocrine therapy)[16–18] since increasing evidence supports that estrogen stimulates malignant proliferation of such cancer cells.[19,20] However, endocrine therapy results in severe side effects because of the extensive role of estrogen systemically.[21–23] Moreover, more than 20% of patients suffer from relapse of cancer after endocrine therapy, and some die of the disease.[24,25] Therefore, new action targets for the treatment of ER$^+$ breast cancer remain an urgent clinical issue to be solved.

Figure 1. Discovery of the active oncogenic enhancer for *c-Myc* in ER⁺ breast cancer cells

(A) Heatmap for screening cancer-associated enhancers by ChIP-seq in MCF-7 cells and MDA-MB-231 cells. The active oncogenic enhancers of MCF-7 cells (ER⁺) and MDA-MB-231 cells (triple-negative) were indicated by cancer-associated signaling pathways and enriched by KEGG analyses. The active oncogenic enhancers were defined

(legend continued on next page)

The oncogene *c-Myc*, which is located at chromosome 8q24,[26,27] is overexpressed in a variety of cancers and plays a critical role in promoting the proliferation of cancer cells.[28–30] Recent studies have revealed that the tissue-specific enhancer of *c-Myc* participates in the development and progression of prostate cancer,[31] colorectal cancer,[32,33] acute myeloid leukemia,[34–36] etc.

c-Myc is one of the key effectors of the estrogen signaling pathway in ER$^+$ breast cancer, and it is associated with the continuous rapid growth of cancer cells after endocrine therapy.[37–39] Nevertheless, the promoter of *c-Myc* has no estrogen-response element.[40] Accordingly, we hypothesize that the regulation of *c-Myc* expression could be induced by estrogen through an estrogen-response enhancer. Therefore, the objectives of this study were to identify the enhancer of *c-Myc*, to verify the function of the enhancer and to reveal the underlying activation mechanism in ER$^+$ breast cancer.

RESULTS

Discovery of the active oncogenic enhancer for c-*Myc* in ER$^+$ breast cancer cells

To understand the regulatory landscape of enhancers in breast cancer, two epigenetic hallmarks of open chromatin, consisting of histone-3 lysine-4 methylation (H3K4me1) and histone-3 lysine-27 acetylation (H3K27ac), were investigated by chromatin immunoprecipitation sequencing (ChIP-seq) in distinct types of human breast cancer cells (ER$^+$ MCF-7 and triple-negative MDA-MB-231), respectively. The active enhancers were indicated by the DNA sequence overlapping with H3K4me1 and H3K27ac signals, while the density of the H3K27ac signal was used to indicate the activity of enhancers.[41] The pathway analysis demonstrated that active enhancers in two cells were highly associated with cancer-related pathways, including the adenosine monophosphate-activated protein kinase (AMPK) signaling pathway, central carbon metabolism in cancer, DNA replication, etc. (Figure 1A).

Further observation showed that the most pathways were correlated with *c-Myc*-related pathways (Figure 1B). Moreover, the relevance of *c-Myc*-related pathways in ER$^+$ breast cancer cells (MCF-7) was much higher than that in triple-negative breast cancer cells (MDA-MB-231). This indicated that the genes in *c-Myc*-related pathways had active enhancers in MCF-7 cells.

Then, the regulatory landscape of the oncogene *c-Myc* was investigated by the UCSC genome browser. The H3K4me1 and H3K27ac signals were remarkably enriched ~65 kb upstream of *c-Myc* in MCF-7 cells, indicating that this region contained a candidate active enhancer of *c-Myc* in MCF-7 cells (Figure 1B). Moreover, the signals in the same region were not enriched in MDA-MB-231 cells, suggesting that this region did not contain the active enhancer in MDA-MB-231 cells (Figure 1B).

In addition, the results from H3K27ac ChIP-seq of three other kinds of ER$^+$ breast cancer cells (BT-549, MDA-MB-468, and ZR-75-1) showed that the candidate region was a common active enhancer of *c-Myc* (Table S1).

To further identify the function of this region, several sequencing datasets were employed from the public database. Based on the *cis*-regulatory function of RNA-Pol II,[42] the RNA Pol II chromatin interaction analysis using paired end tag sequencing (ChIA-PET) in MCF-7 cells was processed in the UCSC genome browser. The peaks of RNA Pol II were found in the candidate region, indicating that this region may regulate the coding region of *c-Myc* by connecting with a DNA loop containing RNA Pol II (Figure 1C). In addition, DNase I hypersensitivity peak clusters in the UCSC genome browser confirmed that the candidate region played a transcription function (Figure 1C). More interestingly, the Vertebrate Multiz Alignment & Conservation (100 Species) track in the UCSC genome browser showed that this candidate region was a highly conserved noncoding genomic region across different species, including rhesus, mouse, and dog. The results showed that this candidate region carried important gene regulatory information during evolution (Figure 1C). These sequencing data further suggested that the candidate region contained an active enhancer of *c-Myc* in ER$^+$ breast cancer cells.
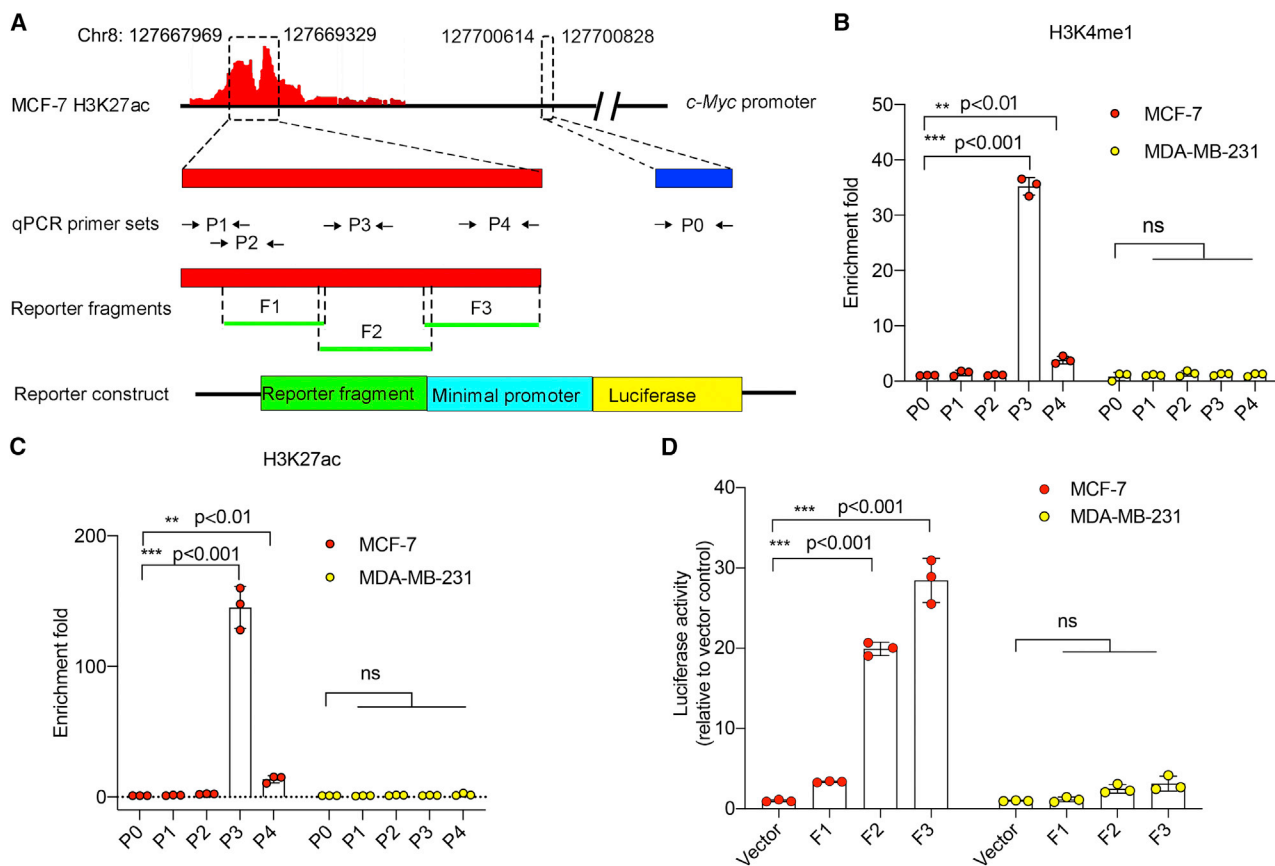
Verification of the active oncogenic enhancer αE_{myc} in ER$^+$ breast cancer cells

To verify the function of the active enhancer, ChIP-quantitative polymerase chain reaction (ChIP-qPCR) was performed on MCF-7 cells and MDA-MB-231 cells. MDA-MB-231 cells were used as the negative control since they lacked H3K4me1 and H3K27ac enrichment around the candidate region. Five primer sets were designed for ChIP-qPCR, among which four primer sets (P1 to P4) were designed to cover the region of the active enhancer, while the remaining primer set (P0) was designed as the negative control at the locus ~30 kb downstream of the candidate region (Figure 2A; Table S2).

The specificity of varying sets of primers was validated by genomic PCR, and then the amplified PCR products were analyzed by agarose gel electrophoresis (AGE). The results showed that the PCR

---

as the overlapping DNA peak areas of H3K4me1 and H3K27ac ChIP-seq. The pathways with p <0.05 were included for investigation. The values in the map were calculated with the negative logarithm of the p value. (B) Differentially active oncogenic enhancers for all genes in *c-Myc*-associated signaling pathways in MCF-7 cells and MDA-MB-231 cells. The difference in active oncogenic enhancers was indicated by the enrichment significance of *c-Myc*-associated signaling pathways. The pathways with a negative logarithm of p ≥3 are highlighted by the green panel. (C) Discovery of an active oncogenic enhancer of *c-Myc* in ER$^+$ breast cancer cells by comparing images in the UCSC genome browser. The promoter and the enhancer of *c-Myc* are highlighted by blue dotted boxes. The candidate active enhancer for *c-Myc* was found only in MCF-7 cells and was predicted by the following tracks: (1) RNA Pol II ChIA-PET data of MCF-7 cells; (2) H3K27ac and H3K4me1 ChIP-seq data of MCF-7(ER$^+$), MDA-MB-231(triple-negative), BT-549 (ER$^+$), MDA-MB-468 (ER$^+$), and ZR-75-1 cells (ER$^+$); (3) DNase I hypersensitivity peak clusters from ENCODE (95 cell types); and (4) genomic conservation across different species (100 species).

**Figure 2. Verification of the active oncogenic enhancer αE_{myc} in ER$^+$ breast cancer cells**

(A) Illustrations of H3K27ac ChIP-seq peaks at the *c-Myc* locus, ChIP-qPCR primer sets and luciferase reporter fragments. Top: magnified view of H3K27ac ChIP-seq peaks at the *c-Myc* locus of MCF-7 cells (ER$^+$). The region of the highest signals of H3K27ac was further magnified (red rectangle). Four primer sets (P1 to P4) for ChIP-qPCR were designed to cover this region. One primer set (P0) for the region without H3K27ac signals was used as the negative control (blue rectangle). Bottom: reporter fragments F1 to F3 (green rectangles) covering primer sets (P2 to P4) were cloned upstream of a minimal luciferase promoter. (B) Enriched H3K27ac at the candidate oncogenic enhancer region in MCF-7 cells (n = 3). (C) Enriched H3K27ac at the candidate oncogenic enhancer region in MCF-7 cells. The studies (B and C) were performed in MCF-7 cells (ER$^+$) and MDA-MB-231 cells (triple-negative) by ChIP-qPCR via primer sets P0 to P5 (n = 3). (D) Enhanced transcription effects of F2 and F3 on the luciferase reporter gene in MCF-7 cells. Each construct was transfected into cells along with a plasmid expressing Renilla luciferase. Luciferase activity was first normalized to Renilla luciferase activity (internal control) and subsequently normalized to an empty vector control (n = 3). Experiments were repeated three times independently. Data are presented as the mean ± standard deviation.

amplification products were of specificity, and the length of each was less than 1,000 bp (Figure S1A).

The target region of P3 and P4 demonstrated significant H3K4me1 and H3K27ac enrichment in MCF-7 cells by ChIP-qPCR, suggesting that the target region of P3 and P4 was an active enhancer in MCF-7 cells (Figures 2B and 2C). Similar to the results from ChIP-seq, there was no signal enrichment of either H3K4me1 or H3K27ac at the candidate region in MDA-MB-231 cells, indicating that this region did not contain the active enhancer in MDA-MB-231 cells (Figures 2B and 2C).

To determine the locus of the active enhancer in the candidate region, a dual-luciferase reporter assay was employed in two distinct types of

cells. Three DNA fragments (F1, F2, and F3) were designed to cover the candidate enhancer region, each of which was 300–500 bp in length (Figure 2A). Their specificity was verified by PCR-AGE (Figure S1B). Then, the DNA fragments were cloned into the firefly luciferase reporter in front of a minimal promoter and verified by DNA sequencing (Figure S2). Afterward, each reporter construct was co-transfected with a pRL Renilla luciferase reporter, which was used to normalize the difference in transfection efficiency in different cells. The results showed that the fragments F2 and F3 enhanced the transcription level of the reporter gene (luciferase) more than 20-fold compared with the control in MCF-7 cells. Similarly, fragment F1 increased the level up to 3-fold (Figure 2D). In contrast, fragments F1, F2 and F3 did not enhance the transcription level of luciferase in MDA-MB-231 cells (Figure 2D). The dual-luciferase reporter assay
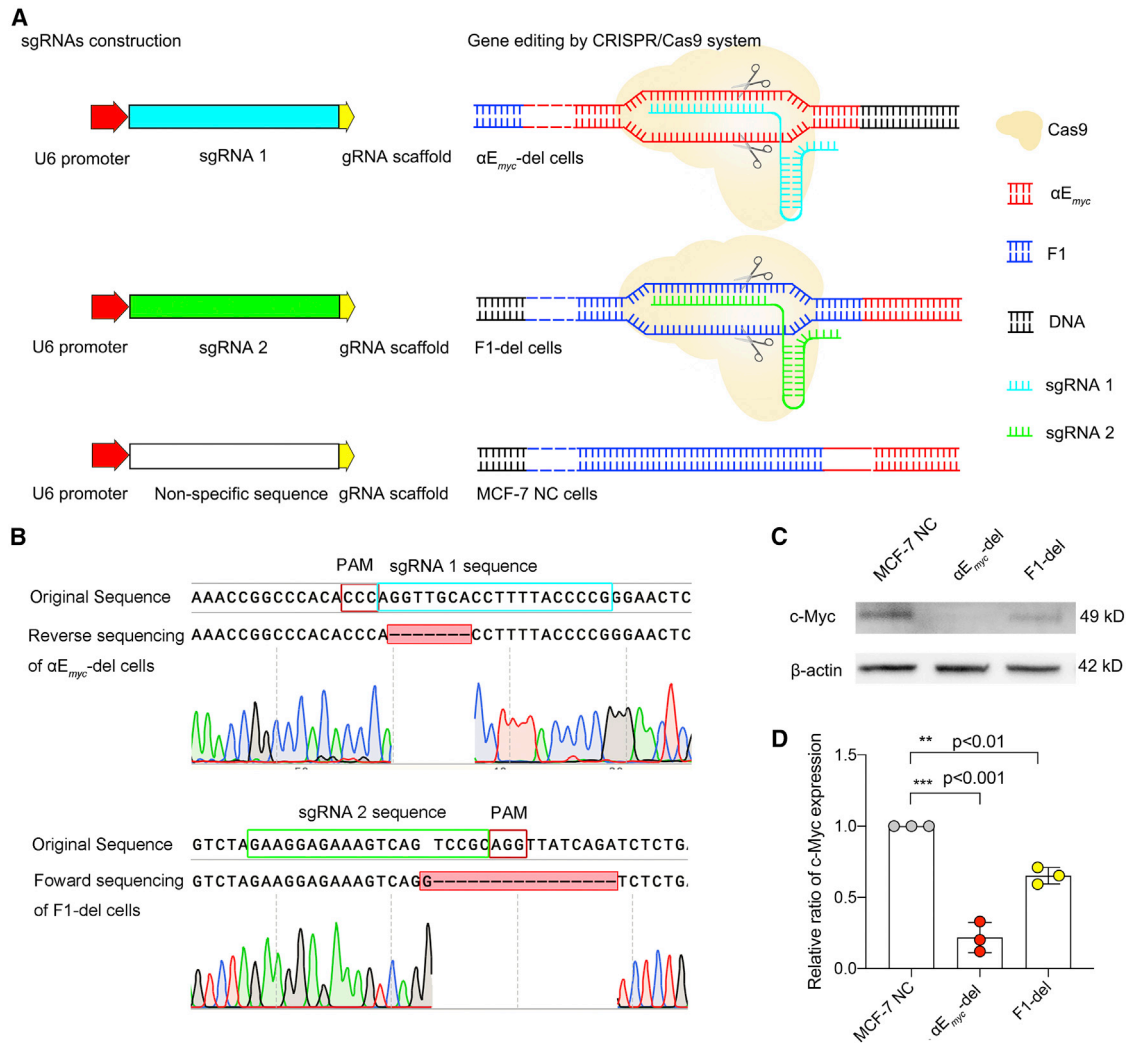
Figure 3. Oncogenic enhancer αE$_{myc}$ promotes the expression of *c-Myc* in ER$^+$ breast cancer cells

(A) Design for deletion of oncogenic enhancer αE$_{myc}$ in MCF-7 cells. Left: illustration of sgRNA construction; right: illustration of gene editing by the CRISPR-Cas9 system. To prepare αE$_{myc}$-del cells, sgRNA 1 was designed to delete the αE$_{myc}$ locus (F2 and F3 fragments); to prepare F1-del cells, sgRNA 2 was designed to delete the F1 fragment; and to prepare MCF-7 NC cells, a nonspecific sequence was designed as the blank control. (B) Verification of αE$_{myc}$ deletion and F1 deletion. DNA sequencing results of αE$_{myc}$-del cells and F1-del cells were aligned to the genome sequence of MCF-7 NC cells. (C) Diminished expression of c-Myc protein in αE$_{myc}$-del and F1-del cells. The study was performed by Western blotting. β-actin was used as the internal reference. (D) Relative ratio of c-Myc protein expression in αE$_{myc}$-del and F1-del cells (n = 3). Quantification of c-Myc protein was performed by ImageJ. Experiments were repeated three times independently. Data are presented as the mean ± standard deviation.

confirmed the active enhancer of *c-Myc* in ER$^+$ MCF-7 cells, and the locus (F2 plus F3 region, 801 bp, at Chr8: 127668529–127669329) was verified as the active enhancer of *c-Myc* (named αE$_{myc}$ afterward; Table S3).

Oncogenic enhancer αE$_{myc}$ promotes the expression of *c-Myc* in ER$^+$ breast cancer cells

To evaluate the enhancing effect of αE$_{myc}$ (F2 plus F3) on the transcription of *c-Myc* in MCF-7 cells, the CRISPR-Cas9 system was employed to delete αE$_{myc}$. MCF-7 cells were infected by lentivirus carrying LentiCRISPR v2 vector encoding sgRNA 1 to form αE$_{myc}$-del cells (targeting αE$_{myc}$) or encoding sgRNA 2 to form F1-del cells (targeting F1) (Figure 3A). In addition, MCF-7 cells infected with lentivirus encoding the LentiCRISPR v2 vector without single guide RNA (sgRNA) were used as the negative control (MCF-7 NC cells) (Figure 3A). The construction of LentiCRISPR v2 vectors was validated by DNA sequencing (Figure S3).

To verify the deletion of targeting sites, genomic PCR and DNA sequencing were employed in the experimental groups. The results revealed a 7-bp deletion in αE$_{myc}$-del cells at αE$_{myc}$, while a 16-bp deletion was found in F1-del cells at F1 (Figure 3B).
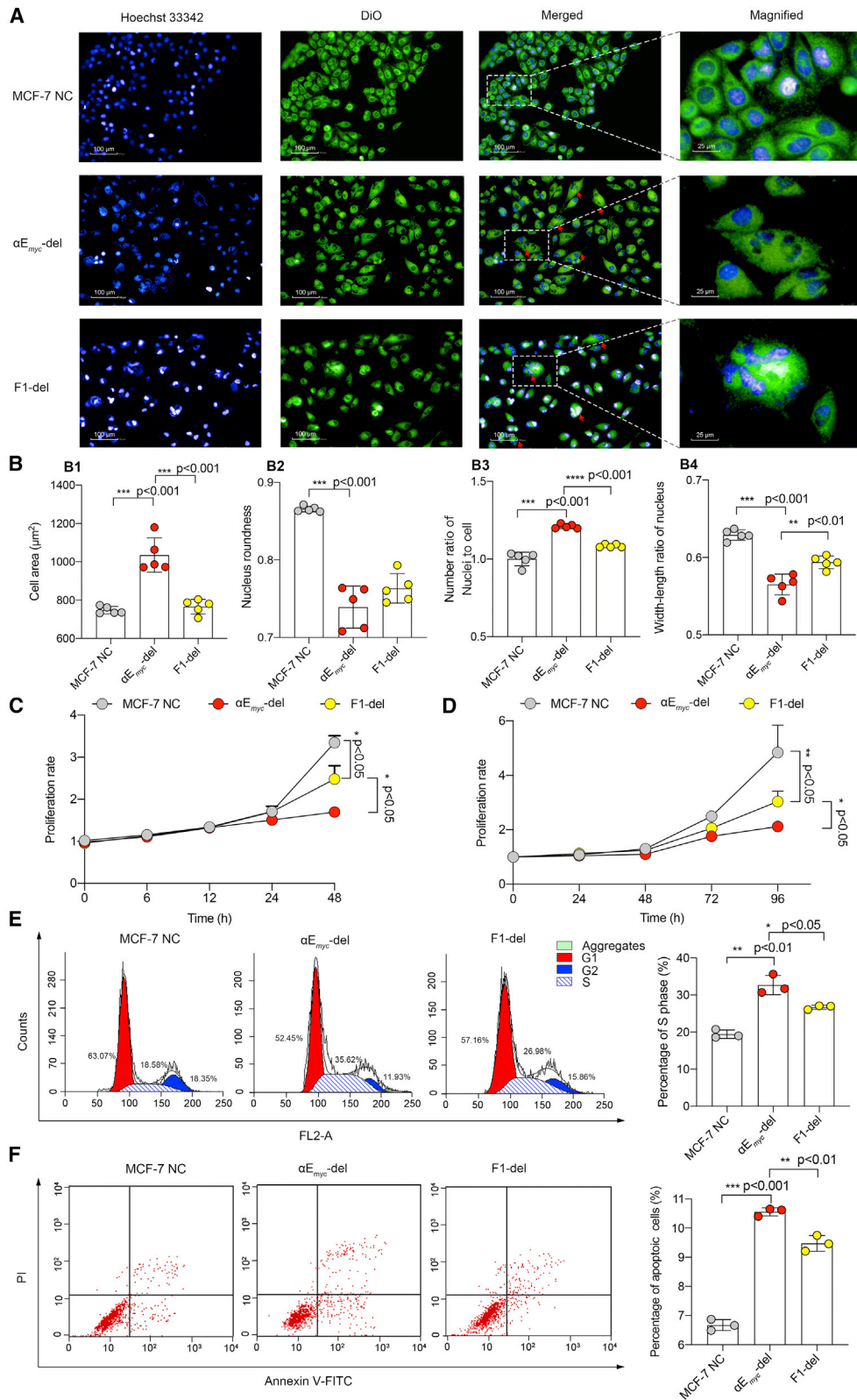
To evaluate the expression of *c-Myc*, qPCR with reverse transcription (qRT-PCR) and Western blotting were employed in the experimental groups. The results showed that the deletion of αE_{myc} led to significant downregulation of *c-Myc* at both the transcriptional (Figure S4) and protein (Figure 3C) levels compared with those in the control. In addition, the deletion of F1 also resulted in the downregulation of *c-Myc* expression at both the transcriptional (Figure S4) and protein (Figure 3C) levels. This result indicated that, as the neighboring region of αE_{myc}, F1 also displayed an enhancing effect on the transcription of *c-Myc*. Nevertheless, the effect of F1 deletion was not as remarkable as that of αE_{myc} deletion (Figure 3D).

Deletion of oncogenic enhancer αE_{myc} impedes the proliferation of ER⁺ breast cancer cells

To investigate the impacts of the oncogenic enhancer on cell morphology, proliferation, cell cycle, and necrosis, αE_{myc} of ER⁺ breast cancer cells was deleted by the designed CRISPR-Cas9 systems. To evaluate the changes in morphological features, images of αE_{myc}-del cells, F1-del cells, and MCF-7 NC cells were captured by a high-content imaging system, and the parameters were quantified, including cell area, nuclear roundness, width-length ratio, and ratio of nuclei to cells. The results showed that the morphological features of the cells changed remarkably after αE_{myc} deletion, consisting of more scattered, size-varied, area-increased, cell roundness-decreased, nucleus roundness-decreased, and polynuclear cells, compared with those of MCF-7 NC cells and F1-del cells (Figures 4A and 4B).

The cell proliferation rates for αE_{myc}-del cells, F1-del cells, and MCF-7 NC cells were measured by a high-content imaging system and CCK-8 assay, respectively. The results from the high-content imaging system showed that the proliferation rate of αE_{myc}-del cells was significantly reduced compared with that of MCF-7 NC cells or F1-del cells (Figures 4C and S5). Moreover, the results from the CCK-8 assay confirmed the inhibitory effect on proliferation after αE_{myc} deletion in MCF-7 cells (Figure 4D).

To observe the effect on the cell cycle, αE_{myc}-del cells, F1-del cells, and MCF-7 NC cells were analyzed by flow cytometry. The results showed that the αE_{myc}-del cells were arrested in S phase compared with MCF-7 NC cells (increased by 13.24% ± 1.64%) or F1-cells (increased by 5.96% ± 1.54%) (Figure 4E). Consequently, αE_{myc}-del cells in G0 and G1 phases were decreased (Figure S6). This phenomenon demonstrated that the period of DNA synthesis in αE_{myc}-del cells was increased significantly.

To measure the effect on cell necrosis, MCF-7 NC cells, αE_{myc}-del cells, and F1-del cells were stained with Annexin V-fluorescein isothiocyanate (FITC)/propidium iodide (PI). During necrosis, the plasma membrane structure was incomplete, and PI entered the cell and stained the nuclei. At the same time, phosphatidylserine (PS) was exposed on the outer leaflet of the plasma membrane in necrotic cells, while the exposed PS was bound with Annexin V-FITC. The results from the flow cytometry showed that the necrotic rate of αE_{myc}-del cells was evidently increased compared with that of MCF-7 NC cells (increased by 3.88% ± 0.14%) or that of F1-del cells (increased by 1.08% ± 0.17%) (Figure 4F). The results demonstrated that deletion of αE_{myc} was able to induce cell necrosis.

Oncogenic enhancer αE_{myc} recruits the transcription factor ERα by estradiol stimulation in ER⁺ breast cancer cells

The above results demonstrated that the deletion of αE_{myc} could inhibit the expression of *c-Myc* in MCF-7 cells (ER⁺) but not in MDA-MB-231 cells (triple-negative). To understand the critical role of ERα in the activity of the αE_{myc} region in MCF-7 cells, the expression of *c-Myc* in two distinct types of cells was investigated after stimulation with estradiol (E2). The results from qRT-PCR and Western blotting showed that E2 was able to stimulate the expression of *c-Myc* in MCF-7 cells compared with the hormone-deprived (HD) control, while the stimulation was effectively blocked by ICI-182780 (ERα antagonist, ICI). In contrast, E2 did not affect the expression of *c-Myc* in MDA-MB-231 cells (Figures 5A and 5B).

It was reported that the promoter of *c-Myc* had no estrogen-response element, and hence, we studied whether the αE_{myc} region had an estrogen-response element. On the one hand, the investigation was performed to observe whether ERα was enriched in the αE_{myc} region. Accordingly, the ChIA-PET data targeting ERα in MCF-7 cells from the public GEO database and our H3K27ac ChIP-seq data in MCF-7 cells were visualized together with the UCSC Genome Browser, and the results of the comparison showed that ERα was enriched in the αE_{myc} region in MCF-7 cells (Figure 5C).

On the other hand, the motif of ERα (the estrogen-response element [ERE]) was predicted by the Jaspar database. The result showed that the complete sequence of ERE was *AGGTCANNNTGACCT* (Figure 5D), and a half-ERE (*TGACCT*) motif was found at the αE_{myc} region (Figure 5E).

Figure 4. Deletion of oncogenic enhancer αE_{myc} impedes the proliferation of ER⁺ breast cancer cells

(A) Changed cell morphology in αE_{myc}-del cells. Representative images were captured by a high-content imaging system. Red arrows, cells with abnormal morphology. Green channel, cellular membrane stained by DiO; blue channel, nuclei stained by Hoechst; merged, a combination of the above channels; and magnified view, 16× folds. Scale bar, 100 or 25 μm (magnified view). (B) Morphology parameters of αE_{myc}-del cells. B1, cell surface area; B2, nucleus roundness; B3, width-length ratio of nucleus; and B4, number ratio of nuclei to cell in MCF-7 NC cells, αE_{myc}-del cells, and F1-del cells, respectively (n = 5). (C) Reduced proliferation of αE_{myc}-del cells. The number of cells was quantified by a high-content imaging system at varying time points. The cell proliferation rate was calculated by normalizing the number of objects at each time point to that at 0 h (n = 5). (D) Reduced proliferation of αE_{myc}-del cells verified by CCK-8 assay. The viability of cells was measured at varying time points. The cell proliferation rates were calculated by normalizing the viability at each time point to that at 0 h (n = 5). (E) Cell-cycle arrest of αE_{myc}-del cells (n = 3). (F) Cell apoptosis of αE_{myc}-del cells (n = 3). The studies (E and F) were performed by flow cytometry. Experiments were repeated three times independently. Data are presented as the mean ± standard deviation.
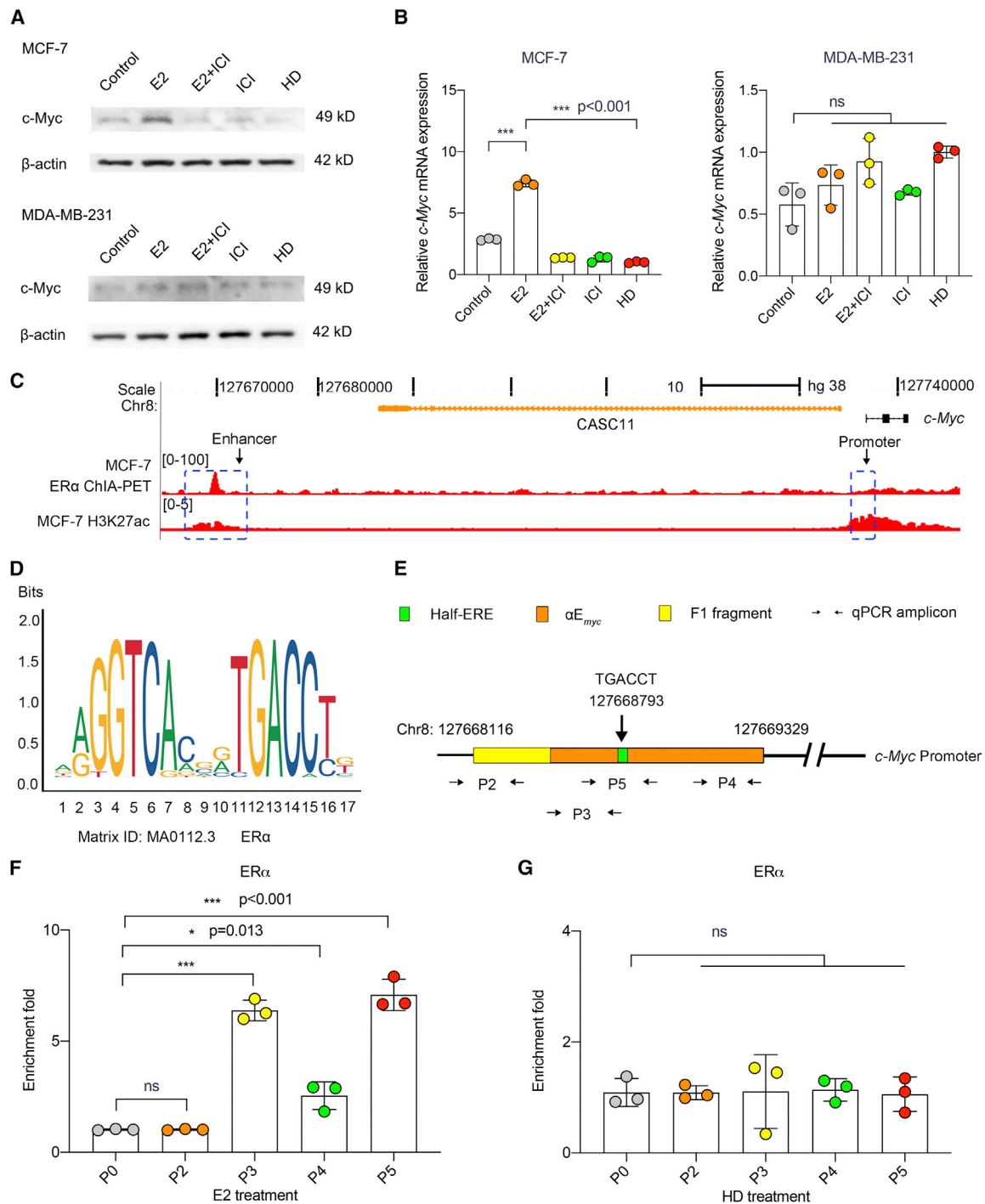
Figure 5. Oncogenic enhancer αE_{myc} recruits the transcription factor ERα by estradiol regulation in ER$^+$ breast cancer cells

(A) Enhanced expression of c-Myc protein by estradiol regulation in MCF-7 cells. β-actin was used as the internal reference. The study was performed by Western blotting. (B) Enhanced expression of *c-Myc* mRNA by estradiol regulation in MCF-7 cells. In (A and B) assays, MCF-7 cells (ER$^+$) and MDA-MB-231 cells (triple-negative) were treated with hormone-free culture medium containing E2, E2 + ICI, ICI, or vehicle. Normal medium- and vehicle-treated cells (A and B) served as the controls. The study was performed by qRT-PCR (n = 3). (C) Enriched transcription factor ERα at the enhancer αE_{myc} locus in MCF-7 cells. ChIA-PET data of ERα in MCF-7 cells (ER$^+$) and H3K27ac ChIP-seq data in MCF-7 (ER$^+$) cells were visualized by UCSC Genome Browser at the *c-Myc* locus. (D) Motif of the ERα binding site. The prediction was performed by JASPAR. (E) Illustration of

(legend continued on next page)

To investigate whether the half ERE was bound to ERα in MCF-7 cells, primer set P5 was designed for ChIP-qPCR, covering the half ERE (Figure 5E). Then, primer sets (P0, P2, P3, P4, and P5) were used to evaluate the enrichment of ERα at the αE_{myc} region in the E2-treated MCF-7 cells and in the HD MCF-7 cells. The results from ChIP-qPCR demonstrated that the target regions of P3 and P5 had high ERα enrichment after E2 treatment, and the target region of both P3 and P5 covered the sequence region of the half ERE (Figure 5F). In contrast, the half ERE was not bound to ERα after hormone deprivation (Figure 5G).

The above fact demonstrated that under the stimulation of estradiol, αE_{myc} recruited the transcription factor ERα through a half ERE in ER$^+$ breast cancer cells.

Activation mechanism of the oncogenic enhancer αE_{myc} in ER$^+$ breast cancer cells

To understand whether the activation of αE_{myc} relied on the coupling of ERα with a half ERE, a CRISPR-dCas9-KRAB system was designed to block the half ERE at the αE_{myc} region. MCF-7 cells were infected with lentivirus carrying the FLAG-dCas9-KRAB vector encoding sgRNA 3, which targeted half ERE (treated with dCas9-sgRNA 3). In addition, MCF-7 cells infected with lentivirus carrying the FLAG-dCas9-KRAB vector, but without sgRNA, were used as the NC (dCas9-vector treated). Infected cells were selected by puromycin, further treated with E2, and finally analyzed by ChIP-qPCR or Western blotting (Figure 6A).

The results from ChIP-qPCR performed on dCas9-sgRNA 3-treated cells showed that the FLAG protein was evidently enriched at the target region of P5 (the half ERE), but ERα was not enriched at the same locus (Figures 6B and 6C). In addition, the results from Western blotting performed on dCas9-sgRNA 3-treated cells and on dCas9-vector-treated cells indicated that the FLAG-dCas9-KRAB fusion protein was expressed in both treated cells (Figure 6D). This fact demonstrated that when the half ERE was occupied by FLAG-dCas9-KRAB, the binding of half ERE with ERα was effectively blocked (Figures 6B and 6C).

To investigate the activity of αE_{myc} after half-ERE blocking, ChIP-qPCR was performed on dCas9 vector-treated cells and on dCas9-sgRNA 3-treated cells. The results showed that H3K27ac was significantly enriched at the half ERE (P5) in dCas9 vector-treated cells compared with the negative region (P0). However, H3K27ac was not enriched at the half ERE (P5) in dCas9-sgRNA 3-treated cells (Figure 6E), demonstrating that the blockage of half ERE significantly reduced the activity of the oncogenic enhancer αE_{myc}.

To observe whether αE_{myc} had a transcription-enhancing effect after half-ERE blocking, qRT-PCR and Western blotting were performed on dCas9-sgRNA 3-treated cells and on dCas9 vector-treated cells to measure the expression of c-Myc, respectively. The results showed that the expression of c-Myc at both the mRNA (Figure S7) and protein levels (Figure 6D) was significantly decreased in dCas9-sgRNA 3-treated cells compared with the dCas9 vector-treated cells, demonstrating that half ERE played a critical role in the transcription-enhancing effect of αE_{myc} on c-Myc.

The above results showed that the 7-bp deletion in αE_{myc} by Cas9-sgRNA 1 nearly abolished the expression of c-Myc (Figure 3C), indicating that this 7-bp region was a core region of αE_{myc} and played a crucible role in oncogenic translational function. To investigate whether the 7-bp region deletion would affect the E2-induced ERα recruitment to half ERE, the enrichments of ERα in E2-treated αE_{myc}-del cells and in E2-treated MCF-7 NC cells were explored. The results from ChIP-qPCR showed that ERα was significantly enriched at the half-ERE (P5) in E2-treated MCF-7 NC cells compared with the negative region (P0). In contrast, ERα was not enriched at the half ERE (P5) in E2-treated αE_{myc}-del cells (Figure 6F), demonstrating that deletion of the 7-bp region impaired the E2-induced recruitment of ERα to the half ERE. This phenomenon implied that the 7-bp region was likely bound by other transcription factors (TFs) involved in the recruitment of ERα to half ERE and in the activation of αE_{myc}.

Based on the above results, the activation of αE_{myc} could be described as follows: (1) TFs bound to the 7-bp region; (2) TFs recruited ERα induced by E2 to the half-ERE region; (3) the formed complex further recruited internal mediator and RNA Pol II to form a DNA loop with c-Myc; and (4) αE_{myc} promoted the transcription of c-Myc (Figure 6G).

DISCUSSION

The enhancer is the functional noncoding DNA sequence that enhances the transcription of the target gene. The oncogenic enhancer and its function in the occurrence and progression of cancer have not yet been defined. In this study, we identified a novel oncogenic enhancer (αE_{myc}) for c-Myc in ER$^+$ breast cancer and confirmed an efficient core enhancer site (GGTTGCA) of αE_{myc} for gene therapy of ER$^+$ breast cancer.

As an important TF, c-Myc has been recognized as one of the most vulnerable targets in the treatment of cancer due to its extensive impacts on the full genome. For years, a number of investigations have reported that the downregulation of c-Myc is beneficial for the treatment of cancers, and a variety of regulation strategies have been developed, such as c-Myc transcription inhibition by direct G-quadruplex stabilizers, c-Myc mRNA degradation by antisense oligonucleotides, and c-Myc protein inactivation by small-molecular inhibitors.[43,44]

---

half ERE (green rectangle) at the αE_{myc} locus. The drawing indicates the relative location of the half ERE and ChIP-qPCR primer sets for the F1 (yellow rectangle) and αE_{myc} (orange rectangle) loci. (F) Enrichment of the transcription factor ERα at half ERE in estradiol-treated MCF-7 cells (n = 3). (G) Deprived enrichment of the transcription factor ERα at half ERE in hormone-deprived (HD) MCF-7 cells (n = 3). The studies (F and G) were performed by ChIP-qPCR via primers P0 and P2 to P5, respectively. Experiments were repeated three times independently. Data are presented as the mean ± standard deviation.
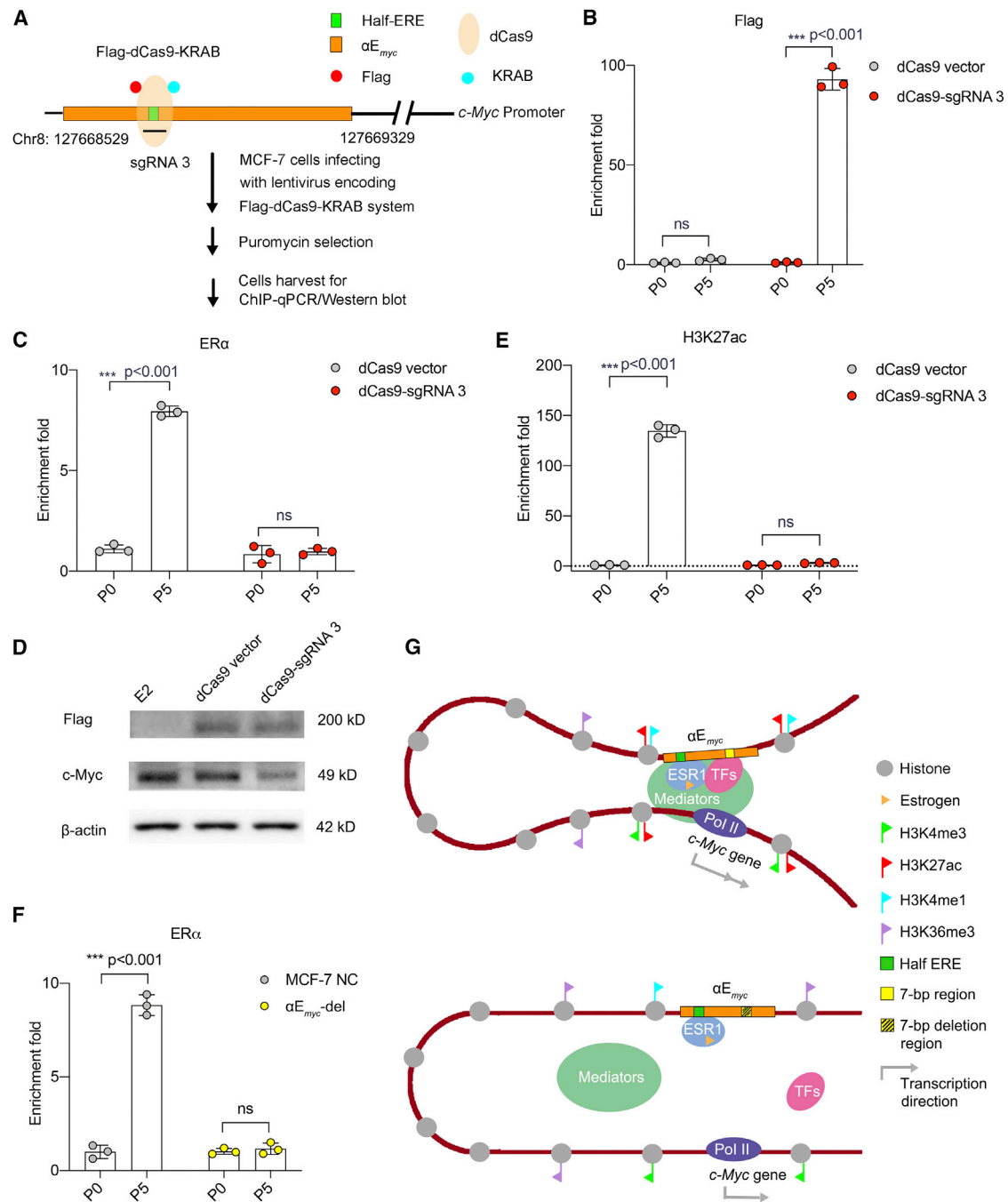
Figure 6. Activation mechanism of the oncogenic enhancer αE_{myc} in ER$^+$ breast cancer cells

(A) Illustration of the inhibition of half ERE by the CRISPR-dCas9-KRAB system in MCF-7 cells. MCF-7 cells (ER$^+$) were infected with lentivirus encoding the FLAG-dCas9-KRAB system, selected by puromycin, and further treated with estradiol (E2) for 30 min for ChIP-qPCR or 6 h for Western blotting. (B) Enriched FLAG protein at half ERE in dCas9-sgRNA 3-treated MCF-7 cells (n = 3). (C) Deprived enrichment of ESR1 at half ERE in dCas9-sgRNA 3-treated MCF-7 cells (n = 3). (D) Expressions of FLAG protein and c-Myc protein in dCas9-sgRNA 3- or dCas9 vector-treated MCF-7 cells. The study was performed by Western blotting. β-actin was used as the internal reference. (E) Deprived enrichment of H3K27ac at half ERE in dCas9-sgRNA 3-treated MCF-7 cells (n = 3). (F) Deprived enrichment of ERα at half ERE in αE_{myc}-del cells. The studies (B, C, E, and F) were performed by ChIP-qPCR via primers P0 or P5 (n = 3). (G) The activation mechanism of the oncogenic enhancer αE_{myc}. The activation could involve the following process: (1) TFs bound to the 7-bp region; (2) TFs recruited ERα induced by E2 to the half-ERE region; (3) the formed complex further recruited internal mediator and RNA Pol II in forming a DNA loop with *c-Myc*; and (4) αE_{myc} promoted the transcription of *c-Myc*. Experiments were repeated three times independently. Data are presented as the mean ± standard deviation.

However, these strategies require sustainable exposure to drugs or continued drug administration to reduce the persistent expression of *c-Myc*. Here, we report a new strategy that disrupts αE$_{myc}$ by gene-editing technology. This strategy achieves significant sustained downregulation of *c-Myc* and ensures the integrity of *c-Myc* at the same time, since *c-Myc* is an essential regulator in cells. Moreover, we demonstrate that this strategy achieves remarkable efficacy for the treatment of cancer.

Approaches to identify enhancers that have been typically applied include (1) ChIP-seq of H3K4me1 and H3K27ac[45] and (2) DNase-seq, which can reveal open chromatin regions.[46] Although these methods are able to yield thousands of candidate enhancers, the candidate enhancers require further verification by experiments. In this study, we first performed ChIP-seq of H3K4me1 and H3K27ac in ER⁺ breast cancer cells and discovered a candidate active enhancer of *c-Myc*. To identify the key enhancer region and to verify the function of the enhancer, ChIP-qPCR and dual-luciferase assays were employed. We reveal that the key enhancer region αE$_{myc}$ could enhance the transcription of downstream genes more than 20-fold. To further investigate the transcription-enhancing effect of the enhancer on *c-Myc* expression, the CRISPR-Cas9 system was used to delete the enhancer. We further elucidate that the deletion of αE$_{myc}$ is able to inhibit the expression of *c-Myc* at both the mRNA and protein levels. In contrast to the previously reported *c-Myc* enhancer[40] in ER⁺ breast cancer, we identify the pivotal enhancer region (801 bp, at Chr8: 127668529–127669329) as αE$_{myc}$ and reveal for the first time the specific oncogenic enhancer function of αE$_{myc}$ in ER⁺ breast cancer.

c-Myc is involved in a variety of pathways to guide specific gene expression and to regulate biological processes, including the cell cycle, cell proliferation, and cell apoptosis.[39] Accordingly, we demonstrate that the deletion of αE$_{myc}$ downregulates the expression of *c-Myc*, thereby leading to cell nucleus changes, cell-cycle arrest, cell necrosis, and finally inhibition of cell proliferation. Regarding the changes in the nucleus of the cells, the most likely explanation is that an increase in DNA synthesis time during the cell cycle leads to the formation of polynucleus cells in αE$_{myc}$-del cells.

The function of enhancers has high cell/tissue specificity, which is due to the different landscapes of TFs in varying cells. Previous studies have demonstrated that ERα is one of the key TFs in the development of ER⁺ breast cancer.[17] By prediction of the Jaspar database, we revealed the motif of ERα and confirmed a half ERE at the αE$_{myc}$ locus. It has been reported that the coupling of ERα with ERE has high plasticity, which means that complete ERE is not always necessary. Accordingly, we demonstrate that ERα binds to half ERE at the αE$_{myc}$ locus under estrogen stimulation in ER⁺ breast cancer cells by CRISPR-dCas9 and ChIP-qPCR technologies, which is consistent with a previous study.[40] This phenomenon explains why the enhancer αE$_{myc}$ is specific in ER⁺ breast cancer but not in triple-negative breast cancer.

It is known that the activation of enhancers involves many protein machines. In this study, we demonstrate that the recruitment of ERα to half ERE plays an important role in activating αE$_{myc}$. Interestingly, we further demonstrate that the 7-bp region is essential for the recruitment of ERα to half ERE, suggesting that there are other TFs involved in the recruitment of ERα at the 7-bp region of αE$_{myc}$. A previous study indicated that the TF C/EBP homologous protein (CHOP) can bind with an enhancer element (*GGTTGCA*),[47] while this sequence is consistent with that of the 7-bp region in the present study. Such involvement as for whether CHOP is enriched at the 7-bp region of αE$_{myc}$ and takes part in the activation mechanism of αE$_{myc}$ leaves a meaningful clue for future research.

In sum, we discover and confirm a new oncogenic enhancer (named αE$_{myc}$) for *c-Myc* in estrogen-positive breast cancer. αE$_{myc}$ enhances the transcription of downstream genes more than 20-fold. The deletion of the 7-bp core region at αE$_{myc}$ is able to evidently downregulate the expression of *c-Myc*, including its gene, mRNA, and protein, and consequently results in cell nucleus changes, cell-cycle arrest, cell necrosis, and finally, remarkable inhibition of cell proliferation. Moreover, we reveal that the activation of αE$_{myc}$ involves TFs binding with the 7-bp region, followed by the recruitment of ERα to the half-ERE region. In conclusion, the present study discovers a novel oncogenic enhancer αE$_{myc}$ (801 bp, at Chr8: 127668529–127669329) and offers a highly efficient core enhancer locus (*GGTTGCA*) of αE$_{myc}$ for gene therapy of ER⁺ breast cancer.

MATERIALS AND METHODS
Cell lines
Human breast cancer cells (MDA-MB-231 cells and MCF-7 cells) and human embryonic kidney cells (HEK293T cells) were purchased from the Institute of Basic Medical Sciences, Chinese Academy of Medical Sciences (Beijing, China). MDA-MB-231 cells, MCF-7 cells, and HEK293T cells were cultured in Dulbecco's modified Eagle medium (DMEM) supplemented with 10% fetal bovine serum (FBS; PAN, Beijing local agent, Germany), 100 U/mL penicillin, and 100 μg/mL streptomycin (Macgene, Beijing, China) at 37°C under 5% CO_2.

Plasmids
pGL4.23 (plasmid #E8411) and pRL-tk (plasmid #E2241) were purchased from Promega (Beijing local agent, China). The pCMV-VSV-G (plasmid #8454), pMDLg/pRRE (plasmid #12251), pMD2.G (plasmid #12259), psPAX2 (plasmid #12260), LentiCRISPR v2 (plasmid #52961), and FLAG-dCas9-KRAB (plasmid #71236) were purchased from Addgene (Beijing local agent, China).

Drugs and treatment
β-Estradiol (#IE0210, E2) was purchased from Solarbio (Beijing, China). ICI-182780 (#ab120131, ICI) was purchased from Abcam (Beijing local agent, China). The chemicals were dissolved in dimethyl sulfoxide (DMSO), and the final concentrations of E2 and ICI were 10 nM.

Antibodies
Histone H3 (mono methyl K4, H3K4me1) antibody (#ab8895) and histone H3 (acetyl K27, H3K27ac) antibody (#ab4729) were

purchased from Abcam (Beijing local agent, China). ERα antibody (#13258), c-Myc antibody (#5605), FLAG antibody (#14793), rabbit immunoglobulin G (IgG) isotype control (#3900), and β-actin antibody (#4970) were purchased from Cell Signaling Technology (Beijing local agent, China).

ChIP and ChIP-qPCR

To measure the targeted DNA fragments bound by specific proteins, ChIP experiments were performed using an EZ-ChIP chromatin immunoprecipitation kit (Merck Millipore #17-371, Beijing local agent, China) according to the manufacturer's protocol. Briefly, approximately 10 million cells were crosslinked with 1% formaldehyde for 10 min at room temperature (25°C) and quenched by the addition of glycine to a final concentration of 125 mM for 5 min. The fixed cells were resuspended in SDS lysis buffer in the presence of protease inhibitor cocktail II and then subjected to 12 cycles (turn on for 20 s and turn off for 10 s) of sonication (Biorupter, Ningbo, China) to generate chromatin fragments of 200–1,000 bp in length. Lysates were centrifuged at $14,000 \times g$ for 10 min at 4°C to remove insoluble material. The supernatant was diluted in ChIP Dilution Buffer. For immunoprecipitation, the diluted chromatin was incubated with NC or specific antibodies overnight at 4°C with constant rotation, followed by incubation with protein G agarose for 1 h. Beads were washed continuously with low-salt immune complex wash buffer, high-salt immune complex wash buffer, LiCl immune complex wash buffer, and Tris-EDTA buffer. Between washes, beads were collected by centrifugation at 4°C. The pulled-down chromatin complex was decrosslinked at 65°C for 5 h in elution buffer. Eluted DNA was digested with RNase at 37°C for 30 min and with proteinase K at 45°C for 2 h for further purification. Purified DNA was enriched by spin columns and analyzed by ChIP-qPCR using specific primers (Table S2). The enrichment fold was calculated by normalizing the specific antibody enriched against the nonspecific IgG-enriched chromatin.

ChIP-seq library construction

To construct the ChIP-seq library, DNA was combined with end repair mix and incubated at 20°C for 30 min. The end-repaired DNA was purified with a QIAquick PCR-purification kit (Qiagen, Beijing local agent, China), and then A-Tailing mix was added and incubated at 37°C for 30 min. The purified adenylate 3′ end DNA, adapter, and ligation mix were combined and incubated at 20°C for 15 min. The adapter-ligated DNA was purified with a QIAquick PCR purification kit. Several rounds of PCR amplification with PCR Primer Cocktail and PCR Master Mix were performed to enrich the adapter-ligated DNA fragments. Then, the PCR products were selected (approximately 100–300 bp, including adaptor sequences) by running a 2% agarose gel to recover the target fragments. The gel was purified with a QIAquick Gel extraction kit (Qiagen, Beijing local agent, China). The final library was quantified in two ways: the average molecule length and sample integrity as well as purity were quantified using an Agilent 2100 bioanalyzer instrument (Agilent DNA 1000 Reagents) and quantified using real-time qPCR.

The double-stranded PCR products were heat denatured and circularized by the splint oligo sequence. The single-strand circle DNA (ssCir DNA) was formulated as the final library. The library was qualified by a Qubit ssDNA kit. The sequencing was performed with the BGISEQ-500 sequencing system, featuring combinatorial probe-anchor synthesis (cPAS) and DNA Nanoballs (DNB) technology for superior data quality (BGI, Shenzhen, China).

Bioinformatics analysis

ChIP-seq raw reads were first filtered to remove low-quality or adaptor sequences by SOAPnuke with the following parameters: filter −1 5 –q 0.5 –n 0.1 –Q 2–5 1 –c 50. Cleaned reads were mapped to the reference genome of NCBI hg38 using SOAPaligner/SOAP2 (v.2.2.5), whose parameters were –v 2 –s 35. MACS2 (v.2.1.2) was used to call peaks (open chromatin regions), in which "—bw 200 –g NCBI –s 50 –p 1e-5 –m 10 30 –broad –B –trackline" was used. The overlapping enrichment peaks between two samples were identified by bedtools intersect mode with an overlap of 50%. KEGG (https://www.kegg.jp/) enrichment of active enhancer regulated genes was performed using phyper (https://en.wikipedia.org/wiki/Hypergeometric_distribution) to calculate the p value, cooperating with the false discovery rate (FDR) by Bonferroni (Table S4).

In silico identification of enhancers

MCF-7 and MDA-MB-231 ChIP-seq data targeting H3K4me1 and H3K27ac were displayed by UCSC Genome Browser. Publicly available ChIA-PET data targeting RNA Pol II in MCF-7 cells and ChIP-seq data targeting H3K27ac in a panel of human breast cancer cell types (accession numbers for the datasets used are listed in Table S1) were downloaded from the GEO database (https://www.ncbi.nlm.nih.gov/geo/) and visualized in UCSC Genome Browser. The Vertebrate Multiz Alignment & Conservation (100 Species) track in the UCSC Genome Browser was employed to identify highly conserved noncoding genomic regions across different species. The DNase I Hypersensitivity Peak Clusters from ENCODE (95 cell types) track in UCSC Genome Browser was employed to identify open chromatin areas.

In silico identification of ERα regulating αE$_{myc}$

MCF-7 ChIA-PET data targeting ERα were processed together with ChIP-seq data targeting H3K27ac by UCSC Genome Browser. The motif of the ERα binding element was predicted by the Jaspar Database.

Enhancer deletion

To delete αE$_{myc}$, sgRNAs targeting the enhancer were designed by Guide Design Resources (https://zlab.bio/guide-design-resources). Then, sgRNAs were cloned into the LentiCRISPR v2 vector using the restriction enzyme BsmB I digestion method and confirmed by DNA sequencing (Tsingke, Beijing, China). The primers are listed in Table S2. HEK293T cells grown to 75% confluency on a 10-cm dish were transfected in DMEM culture medium with 5 μg LentiCRISPR v2 vectors containing sgRNA, 1 μg pCMV-VSV-G, and 200 ng pMDLg/pRRE. After 12 h of culture, the medium was

replaced with fresh complete medium. Viral supernatant was collected at 48 and 72 h posttransfection and concentrated by PEG 8000. MCF-7 cells were infected with concentrated lentivirus encoding the CRISPR-Cas9 system (with verifying designed sgRNAs) in the presence of 4 mg/mL polybrene (Merck Millipore, Beijing local agent, China). After selection with 1 μg/mL puromycin for 2 weeks, cells were single-cell sorted into 96-well culture plates with infinite dilution. Expanded cells were further verified by genomic PCR and Western blotting.

Half-ERE blockade by the CRISPR-dCas9-KRAB system

To block the half-ERE site of the αE_{myc} region, FLAG-dCas9-KRAB vectors were constructed in the same way as LentiCRISPR v2 vectors. Briefly, for lentivirus packaging (encoding the CRISPR-dCas9-KRAB system), HEK293T cells grown to 75% confluency on a 10-cm dish were transfected in DMEM with 2.5 μg FLAG-dCas9-KRAB damping vectors, along with 0.5 μg pMD2. G and 2 μg psPAX2. After 12 h of culture, the medium was replaced with fresh complete medium. Viral supernatant was collected at 48 and 72 h posttransfection, followed by concentration with PEG 8000. MCF-7 cells were infected with concentrated lentivirus encoding the CRISPR-dCas9-KRAB system in the presence of 4 mg/mL polybrene. After 48 h of culture after infection, the cells were selected with 1 μg/mL puromycin for another 48 h. Furthermore, the cells were treated with E2 for 30 min for ChIP-qPCR or 6 h for Western blotting.

Genomic PCR

To investigate αE_{myc} deletion or F1 deletion, genomic DNA of 5×10^5 cells was extracted from αE_{myc}-del cells, F1-del cells, and MCF-7 NC cells using a Tissue & Cell Genomic DNA Purification Kit (GeneMark, Beijing local agent, China). The concentration of genomic DNA was quantified with a Nano300 microspectrophotometer (YPG-Bio, Beijing, China). The target genomic DNA sequences were amplified using I-5 2× High-Fidelity Master Mix (Tsingke Biotech, Beijing, China) according to the manufacturer's protocol. All primer sets were blasted by NCBI to avoid amplifying nonspecific DNA and are listed in Table S2. PCR amplification was set at 94°C for 5 min and 30 cycles (98°C for 15 s, 55°C for 30 s, and 72°C for 1 min), followed by 72°C for 5 min for a final extension. The PCR products were analyzed by AGE (1.5%, w/v) and confirmed by DNA sequencing.

qRT-PCR and qPCR

Gene-expression transcription levels were determined by qRT-PCR. Total RNA was extracted from 10^6 cells using a TRIzol plus RNA purification kit (Invitrogen, Beijing local agent, China) according to the manufacturer's instructions. The concentration of total RNA was quantified with a Nano300 microspectrophotometer. cDNA was synthesized from the total RNA using PrimeScript RT reagent (Takara Bio, Shiga, Japan) by the qRTPCR system (Applied Biosystems CFX Connect Real-Time PCR Detection System; Bio-Rad, Hercules, CA, USA). Then, cDNA was further amplified by adding specific primers and SYBR Premix Ex Taq II (Takara Bio, Shiga, Japan) and measured by the same qRT-PCR system. The expression levels of the target genes were normalized to the expression of GAPDH mRNA or the NC (IgG) in each sample using the $2^{-\Delta\Delta Ct}$ method. Each experiment was performed in triplicate.

Western blotting

To investigate the expression of target proteins, total proteins were determined by Western blotting assay. Proteins were extracted using Pierce RIPA buffer (Applygen, Beijing, China) supplemented with protease phosphatase inhibitor (Beyotime, Shanghai, China). To collect total proteins, the cell lysates were removed by centrifugation at 12,000 RPM at 4°C for 20 min. Total proteins were quantified using the bicinchoninic acid (BCA) protein assay kit (Beyotime, Shanghai, China) according to the manufacturer's instructions. The total proteins were further separated by sodium dodecyl sulfate-polyacrylamide gel electrophoresis (SDS-PAGE), and the separated proteins were transferred onto polyvinylidene fluoride (PVDF) membranes (Merck-Millipore, Darmstadt, Germany). The blots on PVDF membranes were blocked with 5% BSA in tris-buffered saline with Tween 20 (TBS-T) solution, incubated with the appropriate primary antibodies at 4°C overnight, and further incubated with horseradish peroxidase (HRP)-conjugated secondary antibodies at room temperature (25°C) for 1 h. Afterward, the blots were visualized with Immobilon Western chemiluminescent HRP substrate (Millipore, Burlington, MA, USA), and images were obtained using MiniChemi610 (Sage Creation, Beijing, China). The quantification of blots was performed by ImageJ.

Dual-luciferase reporter assays

To evaluate the enhancement effect of the active enhancer candidate region, DNA fragments (F1 to F3), each 300–500 bp in size, covering 1.2 kb of the H3K27ac peak region were amplified by PCR from human genomic DNA and then cloned into pGL4.23 in front of the minimal promoter. The fragments were cloned using the restriction enzymes XhoI (at the 5′ end) and HindIII (at the 3′ end). For luciferase assays, 3×10^3 cells were seeded in 96-well plates for 24 h before transfection with 50 ng of empty pGL4.23 vector or enhancer pGL4.23 vector plus 1 ng Renilla plasmid pRL-tk for each well. Each vector was transfected into triple wells. After 48 h, the luciferase activity of the cells was assayed using the dual-luciferase reporter assay system (Promega, Beijing local agent, China). Firefly luciferase activity was normalized to Renilla luciferase activity.

Cell-cycle assay

To investigate the cell cycle, MCF-7 NC cells, αE_{myc}-del cells, and F1-del cells were starved for 24 h to synchronize the cell cycle. Then, the cells were harvested, washed, and fixed in ice-cold 75% ethanol overnight at −20°C, followed by incubation with RNase A solution (200 μg/mL) at 37°C for 30 min. Afterward, PI solution (100 μg/mL) was added 5 min before each measurement. The DNA content of the cells was measured using flow cytometry (Becton Dickinson, San Jose, CA, USA) equipped with a 15-mW, 488-nm, air-cooled argon ion laser and analyzed by FlowJoTM software v.7 (Becton Dickinson, San Jose, CA, USA). The results are presented as percentages of cells in G0/1, S, and G2/M phases.

Cell apoptosis

To investigate cell apoptosis, MCF-7 NC cells, αE_{myc}-del cells, and F1-del cells were seeded into 96-well culture plates at a density of 5×10^3 cells per well and allowed to adhere overnight. Cells were harvested, washed, and incubated in 200 μL Annexin V binding buffer containing 4 μL 0.5 mg/mL PI along with 2 μL Annexin V-FITC for 15 min at room temperature (25°C) in the dark. Then, the cells were washed with PBS (pH 7.4) three times and measured by flow cytometry (FCM; FACScan, Becton Dickinson, San Jose, CA, USA) equipped with a 15-mW, 488-nm, air-cooled argon ion laser. Files were collected for 10,000 gated events, and three independent duplicate experiments were conducted.

Cell proliferation

To observe cell proliferation, MCF-7 NC cells, αE_{myc}-del cells, and F1-del cells were seeded into 96-well culture plates at a density of 4×10^3 cells per well and allowed to adhere overnight. Thirty-five fields in the middle of each well were captured at 0, 6, 12, 24, and 48 h by a high-content imaging system, and then the number of objects for each field was counted by digital phase contrast. The number of objects for each well was the sum of 35 fields. The number of objects at a defined time point was normalized to the number of objects at 0 h. Cells were imaged with a $20\times$ objective lens.

To investigate cell proliferation, MCF-7 NC cells, αE_{myc}-del cells, and F1-del cells were seeded into 96-well culture plates at a density of 2×10^3 cells per well and allowed to adhere overnight. Cell viability was separately determined at 0, 24, 48, 72, and 96 h by CCK-8 assay following the manufacturer's instructions. The absorbance of each well was measured using a microplate reader at 450 nm. Relative cell viability was calculated by normalizing the cell viability at defined time points to that at 0 h.

Cell morphology

To understand the morphological features, MCF-7 NC cells, αE_{myc}-del cells, and F1-del cells were seeded into a 96-well culture plate at a density of 5×10^3 cells per well and allowed to adhere overnight. The cells were stained with DiO (DiOC18-3) (5 μM) for 5 min and then stained with Hoechst 33342 (5 μg mL^{-1}) at 4°C for 10 min (protected from light). Morphological features were observed and captured by filter-based imaging at 405 or 488 nm using the high-content imaging system with a $20\times$ objective lens. The quantified parameters of the cells were analyzed with high-content analysis software.

Statistical analysis

Prism 7 (GraphPad, La Jolla, CA, USA) was used for statistical analyses, unless otherwise specified. A two-tailed, unpaired Student's t test was used for comparisons. The results are presented as the mean ± standard deviation. A value of $p < 0.05$ was considered to be statistically significant.

Data availability

The authors declare that all data supporting the results in this study are available within the published paper and its supplemental infor-mation. The raw and analyzed datasets generated within the study are available from the corresponding author upon reasonable request. The ChIP-seq data of MCF-7 and MDA-MB-231 cells used in this study are publicly available in the GEO database under the GSE accession number GEO: GSE180080.

AUTHOR CONTRIBUTIONS

W.L. conceived and supervised the project. C.B., J.D., Y.X., Y.L., P.L., J.L., H.Z., H.G., Y.M., Y.R., J.X., and G.W. completed the experiments. C.B. and J.D. wrote the manuscript. W.L. revised the manuscript. All the authors discussed the results and commented on the manuscript.

DECLARATION OF INTERESTS

The authors declare no competing interests.

REFERENCES

1. Rickels, R., and Shilatifard, A. (2018). Enhancer logic and mechanics in development and disease. Trends Cell Biol. 28, 608–630. https://doi.org/10.1016/j.tcb.2018.04.003.

2. Furlong, E.E.M., and Levine, M. (2018). Developmental enhancers and chromosome topology. Science 361, 1341–1345. https://doi.org/10.1126/science.aau0320.

3. Hnisz, D., Abraham, B.J., Lee, T.I., Lau, A., Saint-André, V., Sigova, A.A., Hoke, H.A., and Young, R.A. (2013). Super-enhancers in the control of cell identity and disease. Cell 155, 934–947. https://doi.org/10.1016/j.cell.2013.09.053.

4. Wang, C., Lee, J.E., Lai, B., Macfarlan, T.S., Xu, S., Zhuang, L., Liu, C., Peng, W., and Ge, K. (2016). Enhancer priming by H3K4 methyltransferase MLL4 controls cell fate transition. Proc. Natl. Acad. Sci. USA 113, 11871–11876. https://doi.org/10.1073/pnas.1606857113.

5. Kaufman, C.K., Mosimann, C., Fan, Z.P., Yang, S., Thomas, A.J., Ablain, J., Tan, J.L., Fogley, R.D., van Rooijen, E., Hagedorn, E.J., et al. (2016). A zebrafish melanoma model reveals emergence of neural crest identity during melanoma initiation. Science 351, aad2197. https://doi.org/10.1126/science.aad2197.

6. Maeshima, K., Stanford, S.M., Hammaker, D., Sacchetti, C., Zeng, L.F., Ai, R., Zhang, V., Boyle, D.L., Aleman Muench, G.R., Feng, G.S., et al. (2016). Abnormal PTPN11 enhancer methylation promotes rheumatoid arthritis fibroblast-like synoviocyte aggressiveness and joint inflammation. JCI Insight 1, e86580. https://doi.org/10.1172/jci.insight.86580.

7. Sur, I., and Taipale, J. (2016). The role of enhancers in cancer. Nat. Rev. Cancer 16, 483–493. https://doi.org/10.1038/nrc.2016.62.

8. Belloucif, Y., and Lobry, C. (2022). Super-enhancers dysregulations in hematological malignancies. Cells 11, 196. https://doi.org/10.3390/cells11020196.

9. Chen, X., Zhang, M., Gan, H., Wang, H., Lee, J.H., Fang, D., Kitange, G.J., He, L., Hu, Z., Parney, I.F., et al. (2018). A novel enhancer regulates MGMT expression and promotes temozolomide resistance in glioblastoma. Nat. Commun. 9, 2949. https://doi.org/10.1038/s41467-018-05373-4.

10. Xie, J.J., Jiang, Y.Y., Jiang, Y., Li, C.Q., Lim, M.C., An, O., Mayakonda, A., Ding, L.W., Long, L., Sun, C., et al. (2018). Super-enhancer-driven long non-coding RNA LINC01503, regulated by TP63, is over-expressed and oncogenic in squamous cell carcinoma. Gastroenterology *154*, 2137–2151.e1. https://doi.org/10.1053/j.gastro.2018.02.018.

11. Liu, Q., Guo, L., Lou, Z., Xiang, X., and Shao, J. (2022). Super-enhancers and novel therapeutic targets in colorectal cancer. Cell Death Dis. *13*, 228. https://doi.org/10.1038/s41419-022-04673-4.

12. Sung, H., Ferlay, J., Siegel, R.L., Laversanne, M., Soerjomataram, I., Jemal, A., and Bray, F. (2021). Global Cancer Statistics 2020: GLOBOCAN estimates of incidence and mortality worldwide for 36 cancers in 185 countries. Cancer J. Clin. *71*, 209–249. https://doi.org/10.3322/caac.21660.

13. Brenton, J.D., Carey, L.A., Ahmed, A.A., and Caldas, C. (2005). Molecular classification and molecular forecasting of breast cancer: ready for clinical application? J. Clin. Oncol. *23*, 7350–7360. https://doi.org/10.1200/JCO.2005.03.3845.

14. Reis-Filho, J.S., and Pusztai, L. (2011). Gene expression profiling in breast cancer: classification, prognostication, and prediction. Lancet *378*, 1812–1823. https://doi.org/10.1016/S0140-6736(11)61539-0.

15. DeSantis, C.E., Ma, J., Gaudet, M.M., Newman, L.A., Miller, K.D., Goding Sauer, A., Jemal, A., and Siegel, R.L. (2019). Breast cancer statistics, 2019. Cancer J. Clin. *69*, 438–451. https://doi.org/10.3322/caac.21583.

16. Waks, A.G., and Winer, E.P. (2019). Breast cancer treatment: a review. JAMA *321*, 288–300. https://doi.org/10.1001/jama.2018.19323.

17. Hanker, A.B., Sudhan, D.R., and Arteaga, C.L. (2020). Overcoming endocrine resistance in breast cancer. Cancer Cell *37*, 496–513. https://doi.org/10.1016/j.ccell.2020.03.009.

18. Bradley, R., Braybrooke, J., Gray, R., Hills, R.K., Liu, Z., Pan, H., Peto, R., Dodwell, D., McGale, P., Taylor, C., et al. (2022). Aromatase inhibitors versus tamoxifen in premenopausal women with oestrogen receptor-positive early-stage breast cancer treated with ovarian suppression: a patient-level meta-analysis of 7030 women from four randomised trials. Lancet Oncol. *23*, 382–392. https://doi.org/10.1016/S1470-2045(21)00758-0.

19. Lønning, P.E., Haynes, B.P., Straume, A.H., Dunbier, A., Helle, H., Knappskog, S., and Dowsett, M. (2011). Exploring breast cancer estrogen disposition: the basis for endocrine manipulation. Clin. Cancer Res. *17*, 4948–4958. https://doi.org/10.1158/1078-0432.CCR-11-0043.

20. Le Romancer, M., Poulard, C., Cohen, P., Sentis, S., Renoir, J.M., and Corbo, L. (2011). Cracking the estrogen receptor's posttranslational code in breast tumors. Endocr. Rev. *32*, 597–622. https://doi.org/10.1210/er.2010-0016.

21. Burstein, H.J., Temin, S., Anderson, H., Buchholz, T.A., Davidson, N.E., Gelmon, K.E., Giordano, S.H., Hudis, C.A., Rowden, D., Solky, A.J., et al. (2014). Adjuvant endocrine therapy for women with hormone receptor-positive breast cancer: american society of clinical oncology clinical practice guideline focused update. J. Clin. Oncol. *32*, 2255–2269. https://doi.org/10.1200/JCO.2013.54.2258.

22. Zwart, W., Terra, H., Linn, S.C., and Schagen, S.B. (2015). Cognitive effects of endocrine therapy for breast cancer: keep calm and carry on? Nat. Rev. Clin. Oncol. *12*, 597–606. https://doi.org/10.1038/nrclinonc.2015.124.

23. Haggstrom, L.R., Vardy, J.L., Carson, E.K., Segara, D., Lim, E., and Kiely, B.E. (2022). Effects of endocrine therapy on cognitive function in patients with breast cancer: a comprehensive review. Cancers *14*, 920. https://doi.org/10.3390/cancers14040920.

24. Howell, A., Cuzick, J., Baum, M., Buzdar, A., Dowsett, M., Forbes, J.F., Hoctin-Boes, G., Houghton, J., Locker, G.Y., and Tobias, J.S.; ATAC Trialists' Group (2005). Results of the ATAC (Arimidex, Tamoxifen, Alone or in Combination) trial after completion of 5 years' adjuvant treatment for breast cancer. Lancet *365*, 60–62. https://doi.org/10.1016/S0140-6736(04)17666-6.

25. Szostakowska, M., Trębińska-Stryjewska, A., Grzybowska, E.A., and Fabisiewicz, A. (2019). Resistance to endocrine therapy in breast cancer: molecular mechanisms and future goals. Breast Cancer Res. Treat. *173*, 489–497. https://doi.org/10.1007/s10549-018-5023-4.

26. Ahmadiyeh, N., Pomerantz, M.M., Grisanzio, C., Herman, P., Jia, L., Almendro, V., He, H.H., Brown, M., Liu, X.S., Davis, M., et al. (2010). 8q24 prostate, breast, and colon cancer risk loci show tissue-specific long-range interaction with MYC. Proc. Natl. Acad. Sci. USA *107*, 9742–9746. https://doi.org/10.1073/pnas.0910668107.

27. Holmes, A.G., Parker, J.B., Sagar, V., Truica, M.I., Soni, P.N., Han, H., Schiltz, G.E., Abdulkadir, S.A., and Chakravarti, D. (2022). A MYC inhibitor selectively alters the MYC and MAX cistromes and modulates the epigenomic landscape to regulate target gene expression. Sci. Adv. *8*, eabh3635. https://doi.org/10.1126/sciadv.abh3635.

28. Stine, Z.E., Walton, Z.E., Altman, B.J., Hsieh, A.L., and Dang, C.V. (2015). MYC, metabolism, and cancer. Cancer Discov. *5*, 1024–1039. https://doi.org/10.1158/2159-8290.CD-15-0507.

29. Dang, C.V. (2012). MYC on the path to cancer. Cell *149*, 22–35. https://doi.org/10.1016/j.cell.2012.03.003.

30. Lin, C.Y., Lovén, J., Rahl, P.B., Paranal, R.M., Burge, C.B., Bradner, J.E., Lee, T.I., and Young, R.A. (2012). Transcriptional amplification in tumor cells with elevated c-Myc. Cell *151*, 56–67. https://doi.org/10.1016/j.cell.2012.08.026.

31. Wasserman, N.F., Aneas, I., and Nobrega, M.A. (2010). An 8q24 gene desert variant associated with prostate cancer risk confers differential in vivo activity to a MYC enhancer. Genome Res. *20*, 1191–1197. https://doi.org/10.1101/gr.105361.110.

32. Ying, Y., Wang, Y., Huang, X., Sun, Y., Zhang, J., Li, M., Zeng, J., Wang, M., Xiao, W., Zhong, L., et al. (2020). Oncogenic HOXB8 is driven by MYC-regulated super-enhancer and potentiates colorectal cancer invasiveness via BACH1. Oncogene *39*, 1004–1017. https://doi.org/10.1038/s41388-019-1013-1.

33. Tu, R., Kang, W., Kang, Y., Chen, Z., Zhang, P., Xiong, X., Ma, J., Du, R.L., and Zhang, C. (2022). c-MYC-USP49-BAG2 axis promotes proliferation and chemoresistance of colorectal cancer cells in vitro. Biochem. Biophys. Res. Commun. *607*, 117–123. https://doi.org/10.1016/j.bbrc.2022.03.138.

34. Herranz, D., Ambesi-Impiombato, A., Palomero, T., Schnell, S.A., Belver, L., Wendorff, A.A., Xu, L., Castillo-Martin, M., Llobet-Navás, D., Cordon-Cardo, C., et al. (2014). A NOTCH1-driven MYC enhancer promotes T cell development, transformation and acute lymphoblastic leukemia. Nat. Med. *20*, 1130–1137. https://doi.org/10.1038/nm.3665.

35. Bahr, C., von Paleske, L., Uslu, V.V., Remeseiro, S., Takayama, N., Ng, S.W., Murison, A., Langenfeld, K., Petretich, M., Scognamiglio, R., et al. (2018). A Myc enhancer cluster regulates normal and leukaemic haematopoietic stem cell hierarchies. Nature *553*, 515–520. https://doi.org/10.1038/nature25193.

36. Ottema, S., Mulet-Lazaro, R., Erpelinck-Verschueren, C., van Herk, S., Havermans, M., Arricibita Varea, A., Vermeulen, M., Beverloo, H.B., Gröschel, S., Haferlach, T., et al. (2021). The leukemic oncogene EVI1 hijacks a MYC super-enhancer by CTCF-facilitated loops. Nat. Commun. *12*, 5679. https://doi.org/10.1038/s41467-021-25862-3.

37. Miller, T.W., Balko, J.M., Ghazoui, Z., Dunbier, A., Anderson, H., Dowsett, M., González-Angulo, A.M., Mills, G.B., Miller, W.R., Wu, H., et al. (2011). A gene expression signature from human breast cancer cells with acquired hormone independence identifies MYC as a mediator of antiestrogen resistance. Clin. Cancer Res. *17*, 2024–2034. https://doi.org/10.1158/1078-0432.CCR-10-2567.

38. McNeil, C.M., Sergio, C.M., Anderson, L.R., Inman, C.K., Eggleton, S.A., Murphy, N.C., Millar, E.K.A., Crea, P., Kench, J.G., Alles, M.C., et al. (2006). c-Myc overexpression and endocrine resistance in breast cancer. J. Steroid Biochem. Mol. Biol. *102*, 147–155. https://doi.org/10.1016/j.jsbmb.2006.09.028.

39. Fallah, Y., Brundage, J., Allegakoen, P., and Shajahan-Haq, A.N. (2017). MYC-driven pathways in breast cancer subtypes. Biomolecules *7*, 53. https://doi.org/10.3390/biom7030053.

40. Wang, C., Mayer, J.A., Mazumdar, A., Fertuck, K., Kim, H., Brown, M., and Brown, P.H. (2011). Estrogen induces c-myc gene expression via an upstream enhancer activated by the estrogen receptor and the AP-1 transcription factor. Mol. Endocrinol. *25*, 1527–1538. https://doi.org/10.1210/me.2011-1037.

41. Kimura, H. (2013). Histone modifications for human epigenome analysis. J. Hum. Genet. *58*, 439–445. https://doi.org/10.1038/jhg.2013.66.

42. Schier, A.C., and Taatjes, D.J. (2020). Structure and mechanism of the RNA polymerase II transcription machinery. Genes Dev. *34*, 465–488. https://doi.org/10.1101/gad.335679.119.

43. Allen-Petersen, B.L., and Sears, R.C. (2019). Mission possible: advances in MYC therapeutic targeting in cancer. BioDrugs *33*, 539–553. https://doi.org/10.1007/s40259-019-00370-5.

44. Jovanović, K.K., Roche-Lestienne, C., Ghobrial, I.M., Facon, T., Quesnel, B., and Manier, S. (2018). Targeting MYC in multiple myeloma. Leukemia *32*, 1295–1306. https://doi.org/10.1038/s41375-018-0036-x.

45. Furey, T.S. (2012). ChIP-seq and beyond: new and improved methodologies to detect and characterize protein-DNA interactions. Nat. Rev. Genet. *13*, 840–852. https://doi.org/10.1038/nrg3306.

46. Chen, A., Chen, D., and Chen, Y. (2018). Advances of DNase-seq for mapping active gene regulatory elements across the genome in animals. Gene *667*, 83–94. https://doi.org/10.1016/j.gene.2018.05.033.

47. Sasaki, K., and Yoshida, H. (2015). Organelle autoregulation-stress responses in the ER, Golgi, mitochondria and lysosome. J. Biochem. *157*, 185–195. https://doi.org/10.1093/jb/mvv010.